PNAS RESEARCH ARTICLE | CHEMISTRY
APPLIED PHYSICAL SCIENCES

Structure making and breaking in electrolyte solutions explained by water energetics

Lucia F. Sedano[a], Luis Carlos Pardo[b,c], Gustavo Madrigal[b,c], Eva G. Noya[d], and Carlos Vega[a,1]

Affiliations are included on p. 9.

Edited by Pablo G. Debenedetti, Princeton University, Princeton, NJ; received November 5, 2025; accepted March 9, 2026

The long-standing classification of ions as water "structure-makers" or "structure-breakers" is fundamentally reevaluated through advanced Molecular Dynamics simulations employing the accurate Madrid-2019 force field. We quantitatively study the local hydration structures of 1 m aqueous solutions of LiCl, NaCl, and KCl (through local entropy and Kullback-Leibler (KL)-divergence analysis). We demonstrate that all ions act as net disruptors of water's tetrahedral network, this change being more severe in solutions with high charge density ions. While hydrogen bonding (HB) is diminished within the first hydration shell (FHS) of ions, it returns to bulk-like levels beyond it. From an energetic viewpoint, water–water interactions in solution are destabilized by about 15% compared to pure water, confirming all ions as "structure-breakers" in this regard. Two factors contribute to the energy loss of water: Roughly half arises from a 5% reduction in the total number of HBs, localized primarily within the ions' hydration shells (plus a small contribution from HB distortion); whereas the other half originates from the destabilization of dipole–dipole correlations beyond the FHS. This latter effect, which scales with ionic charge density, is absent for uncharged solutes. Finally, we identify a correlation between the total energy of water (including the ion–water contribution) in solution and the Jones-Dole B coefficient—a correlation that also holds for divalent cations and hydrophobic solutes. The transition from "structure-maker" to "structure-breaker" (i.e., the change of sign in the B coefficient) occurs near the locus where the total energy of water in the solution is similar to that of pure water.

electrolytes | viscosity | structure maker | structure breaker | hydrogen bond

Significance

A prevailing dogma categorizes salts as structure-makers or structure-breakers to explain transport properties, but this classification lacks a clear molecular origin. Hydrogen bonds (HBs) are lost in the first hydration shell of ions but remain unaltered beyond it. The water–water energy is destabilized due to both HB loss and the disruption of dipole–dipole correlations imposed by the electric field of ions. When including the water-ion contribution, we find a universal correlation between the energy change of water in solution (compared to pure water) and the sign of the empirical Jones–Dole coefficient (which indicates the increase or decrease in dilute solution's viscosity compared to pure water). This correlation includes monovalent and divalent cations as well as hydrophobic solutes.

Electrolyte solutions constitute the medium for all biological and geological processes. It is therefore of the utmost interest to gain an understanding of their properties. Lithium plays a critical role in neural synapsis (1), while sodium and potassium are essential for muscle contraction (2, 3). Furthermore, the concentration and distribution of these ions, facilitated by sodium/potassium pumps, have been identified as key factors in cellular specialization (4, 5). Experimental studies on electrolyte solutions are extensive, providing valuable ion–water distance measurements (6–19). The study of aqueous electrolyte solutions has been approached through various vibrational spectroscopic techniques. Conventional infrared and Raman spectroscopy enable observation of changes in O-H vibration modes of water, although numerous experimental techniques show minimal perturbations of water structure by anions, making it challenging to obtain direct molecular-level information (20). Ultrafast nonlinear spectroscopies have proven particularly valuable for probing vibrational energy dynamics in hydrogen-bonded liquids (21, 22). Low-frequency methods such as THz and time-resolved THz-Raman, together with correlated vibrational spectroscopy (CVS), provide insights into how ions modify water–water hydrogen bonds (23, 24). Computer simulations provide microscopic information of the structure of water around different ions, which can help elucidate the complex behavior of these solutions (25–32). When considering electrolyte force fields, the system can be treated either classically, with (33–35) or without (36–41) polarizability inclusion [even force-fields without charge have been proposed (42, 43)]; or by quantum mechanics. The computational cost of treating these systems fully quantum poses an impossibility, so either density functional theory approaches (27, 44–46), quantum-mechanics/molecular-mechanics techniques (47–49) or many-body energy theoretical frameworks (30) are employed instead. Each of these approximations may lead to different results for the same system. In fact, Varma and Rempe showed that even the coordination number of water molecules around an alkali ion, which is a relatively simple and straightforward property, considerably differs depending on the simulation approach and potential, as well as on the selected experimental technique (45). In this

Author contributions: L.C.P., E.G.N., and C.V. designed research; L.F.S. and C.V. performed research; L.F.S., L.C.P., G.M., E.G.N., and C.V. analyzed data; and L.F.S., E.G.N., and C.V. wrote the paper.

The authors declare no competing interest.

This article is a PNAS Direct Submission.

[1]To whom correspondence may be addressed. Email: cvega@ucm.es.

This article contains supporting information online at https://www.pnas.org/lookup/suppl/doi:10.1073/pnas.2531352123/-/DCSupplemental.

Published April 15, 2026.

work we have used the classic nonpolarizable force-field Madrid-2019 (36), which assigns partial charges to the ions in the solution. The conceptualization of this approach is to account for charge transfer between water and the dissolved ions in a mean-field approximation, an idea first introduced by Leontyev and Stuchebrukhov (50, 51) and further supported by other authors (36–38, 52–57) as well as by quantum calculations (46, 58). This model reproduces the densities of the solutions up to their solubility limit, overcoming the common shortage of empirical models of yielding too low solubilities (59). The model accurately describes the maximum in density of electrolyte solutions, a property that is sensitive to the detailed balance between water–water, ion–ion, and ion–water interactions (60, 61). It also provides very precise estimates for the freezing point depression (62). The equation of state and the compressibility are well captured by the model up to 1 kbar in the temperature range where experiments are available; and in terms of transport properties, this electrolyte model has been shown to capture an anomalous increase in the diffusion of water in the supercooled regime (63), in accordance with some experimental results (64).

The persistence of the structure-maker/breaker dichotomy (11, 65), despite its limitations, can be traced to its intuitive appeal and historical roots in the work of Cox and Wolfenden (66) and Gurney (67). The quest for a unified and simplified behavior of ionic solutions led to a vague link between "structure" and the Hofmeister series, which ranked ions by their ability to precipitate proteins (the "salting-out" effect) (68). Subsequent work (31, 69–73) sought to connect ion-induced structural changes (e.g., radial distribution functions) with dynamic properties like viscosity and residence times, as well as thermodynamic quantities such as hydration entropy and enthalpy. Interestingly, the detailed hydrogen bond network of solutions has received far less attention (74–78). While these terms intuitively suggest that ions either enhance or disrupt water's hydrogen-bond network, the actual structural consequences have been difficult to quantify. Recent work has shifted focus to how ions affect water's dipole correlations, providing a more rigorous framework (79). This perspective explains the well-known concentration-dependent decrease in dielectric constant through disrupted long-range water ordering rather than just local electrostriction effects.

Our current work addresses a fundamental gap in understanding the relationship between structural perturbations and dynamic properties in electrolyte solutions. We establish a correlation between the change in the intermolecular water energy (relative to pure water) and the Jones-Dole viscosity coefficient, B (80). B is positive for electrolytes that increase the viscosity of water and negative otherwise. Experiments (81) show that the diffusion coefficient of water is inversely related to the viscosity of the solution: Increasing the viscosity relative to pure water decreases the diffusion coefficient and vice versa. Since both magnitudes are anticorrelated, our correlation for the viscosity (*via* the B coefficient) can also be used to understand the dynamics of water. Interestingly, the change of sign in B (i.e. the frontier between structure makers and structure breakers) occurs for salts for which the total energy of water (including ion–water interactions) in the solution is comparable to that of pure water.

Results

Before presenting structural results, the force field's validity for ions and water must be assessed. While no classical model perfectly reproduces all properties, key features like the temperature of maximum density (TMD) of water (277 K at ambient pressure) must be accurate. Salts systematically lower the TMD by 4 to 15 K at 1 molal (60), as first shown by Despretz (82), reflecting ion disruption of water's structure.

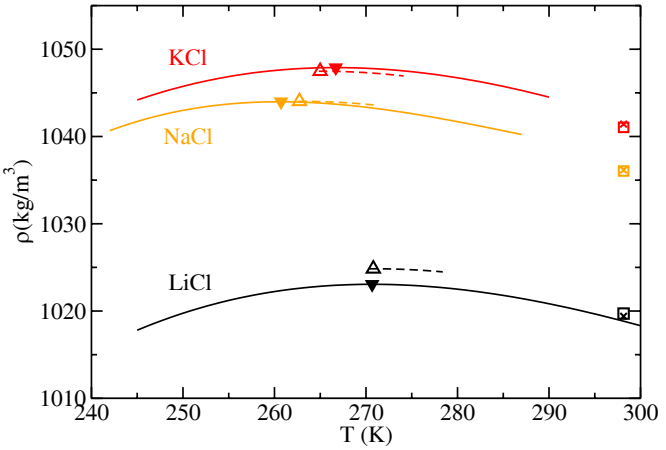

Fig. 1. Density for various chloride solutions at 1 m as a function of temperature at 1 bar from ref. 60. Solid lines: simulations for the Madrid-2019 model. Dashed lines: experiment. Triangle: TMD; empty: experiment, filled: simulation. Experimental density at 298.15 K (square from ref. 60, cross from ref. 83).

Fig. 1 compares experimental and simulated TMDs for 1 molal LiCl, NaCl, and KCl solutions from ref. 60. The close agreement supports the force field's reliability for structural studies.

Structure of Ions Around Water. The location of the first minimum of the Radial Distribution Function (RDF) between the ion and the water's oxygen (*SI Appendix*, Table S1) delimits the first hydration shell (FHS). We shall refer to the water molecules within this limit as hydrated, and those beyond it as free.

Fig. 2*A*, shows the axis definition, where the cosine of the angle θ formed between the vector from the oxygen of a water molecule to an ion belonging to its first hydration shell (FHS), and the dipole moment μ of the water molecule located at the bisector formed by the hydrogen atoms is used for computing the probability distribution functions (PDFs) of panel (*C*). Chloride atoms are practically aligned with the vector that goes through the oxygen and hydrogen atoms, deviating only 2° from it. Naturally, the cations are found pointing toward the oxygen atoms, with the probability distribution being narrower as the ion size decreases (the water molecules are more tightly bound to high density charged ions). This is also depicted in panel (*B*) by the Spatial Density Map (SDM), which illustrates the regions around water where it is most probable to find an ion (*SI Appendix*, section S2).

Water Structure Around Ions. To study the structure of water around the ions we have computed two partial RDFs: $g_{OO}^{hyd-hyd}$, which is the oxygen–oxygen RDF (g_{OO}) between hydrated water molecules, and $g_{OO}^{hyd-wat}$ which is the g_{OO} between hydrated water molecules and any other water molecule. These RDFs are depicted in Fig. 3 (*SI Appendix*, Fig. S2), together with the oxygen–oxygen RDF of pure water g_{OO}^{o}, for comparison.

The first observation is that, for all ions, $g_{OO}^{hyd-wat}$ resembles that of bulk water beyond 6 Å (*SI Appendix*, Fig. S2 for g_{OO} up to 10 Å), where the ions should play (almost) no role. However, at short distances there is a departure from bulk water behavior, whose magnitude depends on the ion. For the chloride, only a decrease in the height of the first peak is observed, which can be ascribed to the fact that the ion occupies a space that would

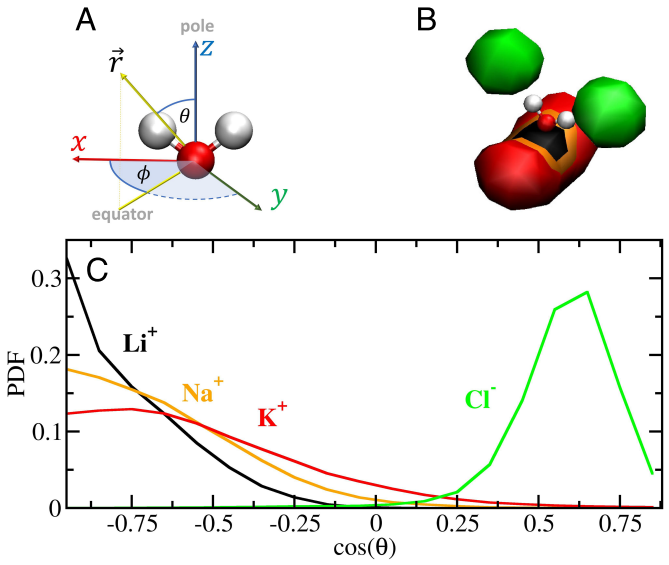

Fig. 2. (*A*) Axis definition for the calculation of position and orientation of neighboring waters or ions around water. The water molecule stands on the XZ plane, and its dipole moment aligns with the Z axis. (*B*) Most probable location of ions [see legend (*C*) for ion identification] around a water molecule (see *SI Appendix*, section S2A for more details). (*C*) Normalized probability distribution of the cosine of the angle θ (bin size 0.1) defined in panel (*A*) at 283 K and 1 bar. Angular distribution function is normalized to 1. The average value of $cos(\theta)$ for Li, Na, K, Cl are −0.77, −0.66, −0.54, 0.58, respectively, which correspond to angles of 140°, 131°, 123°, and 54°.

otherwise correspond to a water molecule, hence yielding a lower probability for the maximum. The spread of FHS water molecules $g_{OO}^{hyd-hyd}$ indicates how strongly water molecules are bonded to the ion in the FHS, being more localized as the density charge of the cation increases, in agreement with previous studies (26, 30). In the case of Cl^-, since the hydrogen atoms point toward the ion, the mobility of the oxygen is greater with an extended range of distances. Consistent with this, Fig. 3*E* demonstrates that almost all hydrogen bonds ($HB^{hyd-hyd}$) are disrupted in the first hydration shell of chloride, with only a small region remaining at negative energies. In Fig. 3*I*, this negative spot is considerably bigger, as it includes the HB between water molecules of the FHS with all others ($HB^{hyd-wat}$).

In contrast, for cations, in addition to the reduction of the first peak's height, significant changes are observed at larger distances as well. For potassium, the number of $HB^{hyd-hyd}$ is significantly larger (Fig. 3*F*) than for the other cations, in good agreement with experimental results (84). It also shows as a pre-peak of the FHS $g_{OO}^{hyd-hyd}$; that is, only the small amount of water molecules within the FHS that are able to form HB are located at small distances. In the case of Na^+, this distribution is no longer bimodal and the maximum of $g_{OO}^{hyd-hyd}$ lies at longer distances, almost coincident with the minimum g_{OO}^{o}, which results in a double peak for the $g_{OO}^{hyd-wat}$: The first peak corresponds to water molecules that form HB (either hydrated-hydrated or hydrated–free), whereas the second peak corresponds to water molecules that cannot establish HB. Finally, the case of lithium is different. The peak is as high as that of pure water and even broader. A glance at the energy panels (*H* and *L*), shows a repulsive energy, which is lacking in pure water (*SI Appendix*, Fig. S7) and no sign of HBs between hydrated water molecules whatsoever.

Since one-dimensional RDFs cannot fully characterize short-range order, we further analyzed the spatial arrangement of water molecules belonging to the FHS. In Fig. 4, the most probable orientation up to 3.3 Å of any water molecule with respect to a water molecule in the FHS is shown (notice that this includes both hydrated and free water molecules). For pure water (Fig. 4 *A*), the central molecule acts as an acceptor (A) at $\cos(\theta) \approx -0.5$ (104°) and $\phi = \pm 90°$, and as a donor (D) at $\cos(\theta) \approx 0.6$ (52°) and $\phi = 0°, \pm 180°$. The spatial distribution for D is narrow (yellow peaks), while A distributions are broader, especially in

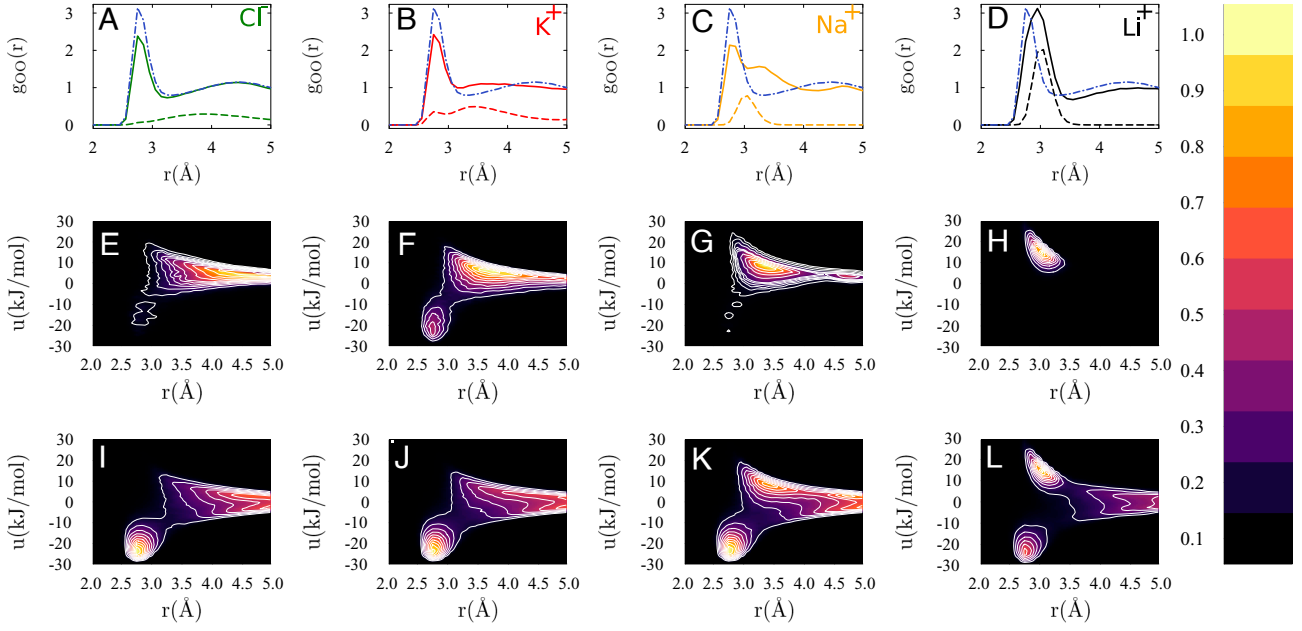

Fig. 3. (*A–D*) Oxygen–oxygen radial distribution functions. Dashed line: RDF for water molecules that belong strictly to the FHS ($g_{OO}^{hyd-hyd}$). Solid line: RDF for molecules of water in the first hydration shell (FHS) of the ions with the rest of water molecules of the system ($g_{OO}^{hyd-wat}$). In blue color we show the RDF of pure water (g_{OO}^{0}) at 238 K and 1 bar. (*E–L*) Bivariate probability distribution function of the water energy, where (*E–H*) correspond to FHS water molecules with each other [dashed lines in panels (*A–D*)] and (*I-L*) correspond to hydrated water molecules with any other water molecule of the system [solid lines in panels (*A-D*)].

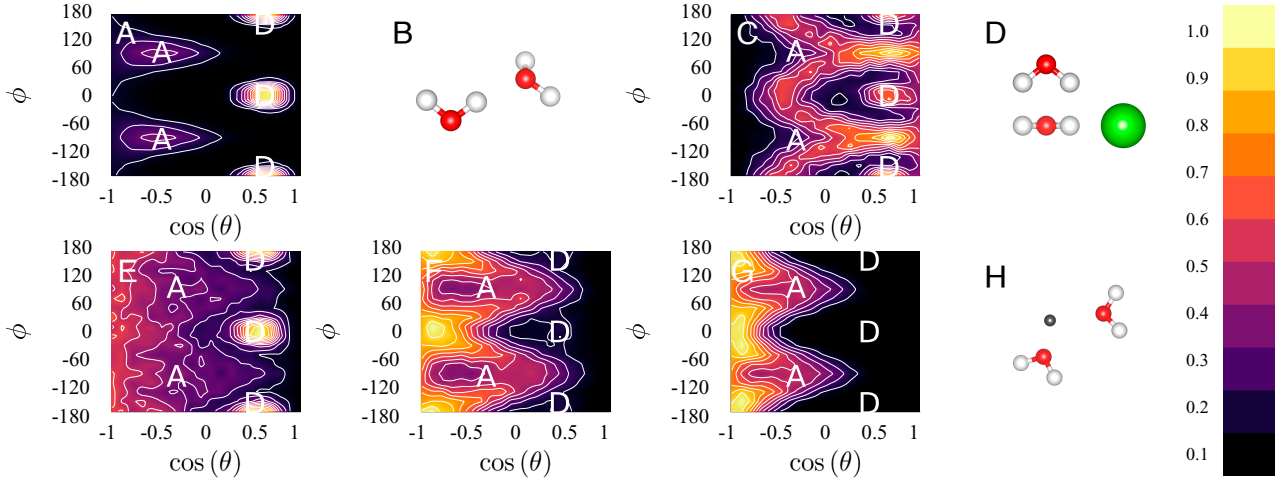

Fig. 4. Normalized probability distribution p(cos θ, ϕ) for oxygen–oxygen atoms of water molecules for distances smaller than 3 Å (following the axis reference system shown in Fig. 2*A*) at 283 K for 1 m solutions. For solutions, the central oxygen belongs to a hydrated water molecule, but the cutoff radius includes hydrated and free water molecules within that reach. The letters D and A denote the angular positions where the central molecule acts as donor or acceptor. (*A*): for pure water. (*B*) Most probable position and orientation of adjoining water molecules (in pure water) from Euler angles probabilities (*SI Appendix*, section S2). (*C*) Same as (*A*) but for water molecules around chloride. (*D*) Most probable position and orientation of adjoining water molecules which are hydrating a chloride ion. (*E*–*G*): Same as (*A*) but for water molecules around potassium, sodium, lithium, respectively. (*H*): Same as (*D*) but for water molecules around lithium.

cos(θ). Since every hydrogen bond donor requires an acceptor, the integral of the D region equals that of the A region in pure water. A peak in the D region guarantees hydrogen bonding—the O-H vector of the central molecule points toward the oxygen of the neighboring water molecule. However, an A region peak only indicates the possibility of hydrogen bonding, as our analysis lacks information about the neighboring molecule's OH vector orientation. Therefore, hydrogen bond quantity is determined by D peak intensity.

Fig. 4 *A* and *B* show the tetrahedral arrangement of pure water, which is increasingly disturbed as the ion's electric field becomes stronger (*E*–*G*). Neighboring water molecules tend to align along the poles of the water dipole, with distinct behaviors for anions and cations. For chloride, a water's hydrogen points toward the anion (as previously shown in Fig. 2), occupying one of the tetrahedral positions of bulk water, and the neighboring molecule can rotate around the O-H axis pointing to the anion. For cations, the water dipole (not the O-H bond) is forced to point outward from the ion, which is found in the antiparallel dipole region, being the molecular reorientation more constrained than for chloride. As previously stated, Cl^- and K^+ are able to form donor HBs (Fig. 4 *C*–*E*), whereas it is not the case for Na^+ and Li^+ (Fig. 4 *F* and *G*). As can be seen in Fig. 4*D* for the chloride, adjacent water molecules show an angle of 90° between dipoles, with their hydrogen atoms confronted, giving rise to the peculiar rings in Fig. 4*C*. In the case of cations (Fig. 4 *E*–*G*), there is a clear imposition of orientational constraints as the size of the cation decreases. To quantify this difference between neat and solution water in the positional maps, we have also calculated the KL-divergence as a function of distance (*SI Appendix*, section S3).

Finally, we compare FHS water molecules to bulk water by computing the local relative entropies up to 6 Å from ions, which are collected in Table 1 (detailed information can be found in *SI Appendix*, section S4). These entropies show negative values, indicating that water is more ordered around ions than it is in pure water. The translational term is small compared to the orientational one, meaning that entropy changes arising from "missing" water molecules in the ion cavity are less important than those driven by active water ordering due to the electric field of ions. Cation entropies show clear size-dependent ordering: Smaller cations cause more distorted water structures.

In Table 2, we present the number of hydrogen bonds according to the Luzar and Chandler criterium (85); namely an O-H ·· O angle smaller than 30° and an oxygen–oxygen distance smaller than 3.3 Å (the first minimum g^o_{OO} at 283 K and 1 bar. See *SI Appendix*, Table S1 and Fig. S1). Results for CsCl using the same force field (55) have been included to illustrate more clearly

Table 1. Local relative entropies (see *SI Appendix*, section S4 for details) calculated up to a distance r_{max} = 6 Å of ions with respect to liquid water at 283 K and 1 bar ($\Delta S^{ex} = S^{ex,ion} - S^{ex,\circ}$ in cal/K·mol)

	ΔS_{trans}	ΔS_{ang}	ΔS_{tot}
Cl^-	0.7	−5.5	−4.8
K^+	0.8	−3.7	−2.9
Na^+	0.5	−5.4	−4.9
Li^+	−0.4	−16.6	−17.0

Table 2. Average number of hydrogen bonds according to the Luzar–Chandler criterion (85) (see text) for 1 m solutions using the Madrid-2019 (36) at 283 K and 1 bar

	LiCl	NaCl	KCl	CsCl	LJ_{KCl}
n_{HB}	3.45	3.44	3.44	3.45	3.65
n_{HB}^{free}	3.64	3.65	3.64	3.64	3.64
n_{HB}^{+}	2.16	2.35	2.59	2.65	3.66
n_{HB}^{-}	2.60	2.59	2.58	2.59	3.65
$n_{HB}^{FHS,+}$	0	0.24	1.27	1.38	11.5
$n_{HB}^{FHS,-}$	0.24	0.26	0.25	0.23	15.3

Pure water (TIP4P/2005) has 3.63 HB. The superscript *FHS* indicates the HB formed between water molecules belonging to the first hydration shell of an ion with each other (the results are not normalized by the coordination number of water for each ion). Superscripts "+" and "–" correspond to water molecules hydrating the cation and anion, respectively, so that $n_{HB}^{+/-}$ denotes the HB formed between a hydrated molecule with any other. n_{HB}^{free} is the HB formed by water molecules that are not hydrating any ion with any other water molecule. LJ_{KCl} is a Lennard-Jones solute molecule (see main text).

the trends with the size of the cation. Furthermore, we introduce a Lennard-Jones solute formed by neutral K and Cl, whose parameters were fitted to reproduce the ion-oxygen distances for K and Cl from the Madrid-2019 model. Since the parameters are fixed to mimic the distances of KCl, we shall denote it as LJ_{KCl}. The net loss of HB in the solutions is independent of the salt and is around 5% (i.e., 3.44 HB in the ionic solutions vs. 3.63 in pure water at 283 K and 1 bar). For the LJ_{KCl}, a slight increase is observed in accordance with the results that Grabowska et al. found in the FHS of methane in water (86). This is a good example of the cage effect for a hydrophobic particle: Water molecules encapsulate the purely LJ atoms (hydrophobic groups) by forming a network of HB around them.

The net loss of hydrogen bonding with respect to pure water in the FHS around the cation (n^{+}_{HB}) ranges from 40% for Li^+ to around 27% for Cs^+. For the anion (n^{-}_{HB}), the decrease is around 28% (without counting the HB formed between water and the chloride). However, beyond the FHS, water maintains the same HBs as pure water (n^{free}_{HB}). Therefore, the loss of HB in solution is strictly due to the water molecules in the first hydration shell because they align with the electric field of the ion. This observation is in good agreement with results found by ab initio molecular dynamics simulations (77, 78, 87) as well as experiments (12, 88, 89). In the case of low charge density ions, such as Cs^+ and K^+, it is still possible to form HBs between the water molecules of the FHS ($n^{FHS,+}_{HB}$). The total number of HBs per ion is approximately 1.38 for Cs^+ and 1.27 for K^+. When this value is divided by the number of water molecules in the cation's hydration shell, each hydrating water molecule forms, on average, 0.2 HBs with each other. Nonetheless, this possibility is reduced for smaller ions and Li^+ does not form any, as previously discussed in Figs. 3 and 4. However, water molecules in the FHS of any ion still engage in HB with free water molecules ($n^{+/-}_{HB}$ in Table 2 and panels *I*–*L* Fig. 3).

In a 1 m NaCl solution there are around 27 molecules of water per ion, forming two complete hydration shells. Due to thermal motion, a small amount of contact ion pairs, and solvent shared ion pairs are generated. In these cases, a water molecule may belong simultaneously to the hydration layer of two ions. In our analysis, this has an occurrence of 1%, 1.5% and 2% for LiCl, NaCl, and KCl, respectively. Consequently, this minor ambiguity does not significantly affect the reported HBs in the hydration shells of ions.

The Impact of Ions on the Water Potential Energy. It is interesting to compare the potential energy of pure water (U^0_{ww}) with the water–water contribution to the potential energy in aqueous solutions (U_{ww}) at 1 m (capital letters indicate that the energy is not divided by the number of water molecules, whereas u_{ww} expresses the molar energy). It can be seen in Table 3 that u_{ww} decreases (in absolute value) when adding salt. The magnitude of the change is significant (16% for LiCl and 13.5% for CsCl). This fact contrasts with the previously discussed loss of only around 5% of HBs. Dissolved ions have two effects: They exclude a certain volume (cavity effect) and they create an electric field. To separate both contributions, we compare with the results for the hydrophobic system (LJ_{KCl}) presented earlier. Table 3 shows that the LJ_{KCl} barely disturbs the water–water energy (it even slightly stabilizes water), nor does it affect the HB (as shown in the previous section). Therefore, even if some of the remaining hydrogen bonds in solution are less energetic due to the distortion caused by ions, that would not explain the huge energy loss between water molecules in the solution (with respect to pure water).

Table 3. Contribution of water–water interactions to the potential energy per molecule of water (u_{ww}) for pure water and for the 1 m electrolyte solutions at 283 K, 1 bar and the Madrid-2019 force-field

	u_{ww}	% Δu_{ww}	$u^{3.3A}_{ww}$	% $\Delta u^{3.3A}_{ww}$
Water	−48.84	0	−36.20	0
LiCl (aq)	−41.04	15.97	−33.59	7.7
NaCl (aq)	−41.36	15.31	−33.60	7.7
KCl (aq)	−42.11	13.77	−33.47	7.5
CsCl (aq)	−42.27	13.42	−33.36	7.8
LJ_{KCl}	−48.88	−0.08	−36.39	−0.5

Results for the hydrophobic LJ_{KCl} are also included (see text). $\Delta\ u_{ww}$ is the percentage change with respect to pure water. $u^{3.3A}_{ww}$ is the energy at 3.3 Å, which corresponds to the first point of Fig. 5*A* for all salts (*SI Appendix*, Fig. S8).

To analyze this issue in more detail, we compute the water–water potential energy up to a certain distance r_c between the water molecules (as defined by the distance between the oxygen atoms). We repeated the calculations for several values of r_c starting at 3.3 Å and ending at 24 Å. For this analysis, we did not use PME, since we are interested in the decay of the energy as a function of the cut-off distance (see *SI Appendix*, section S6 for more details, where results for the other solutions are also depicted).

Given that HBs between water molecules impose distances below 3.3 Å, the energy at this distance is collected in Table 3 as $u^{3.3A}_{ww}$, whereas u_{ww} accounts for the energy at convergence $r \to \infty$, represented by the inclusion of Ewald sums, dashed line in Fig. 5*A*. This figure shows that the difference between u_{ww} (water in solution) and u^0_{ww} (pure water) remains constant for distances greater than 10 Å, which is more clearly depicted in the *Inset* as the derivative of $\Delta u_{ww} = (u_{ww} - u^0_{ww})$ rapidly approaches zero beyond this distance. This is also observed by the short range energy ($u^{3.3A}_{ww}$), which corresponds mainly to the HB network (although it also includes dipole correlations within the FHS) and represents around 75% of the total energy of water. Its loss in 1 m solutions is around 7.5% (5% due to HB breakage and 2.5% to distortion), whereas $u^{r\to\infty}_{ww}$ is around 15%. Therefore, the remaining half of the energy loss for water–water interactions in solution is found in the intermediate 3.3 to 10 Å region, which roughly corresponds to the second and third solvation shells. This arises mainly from the disruption of dipole–dipole correlations (and also, although to a lesser extent, from higher multipole coulombic energies), which is also the origin of the reduction of the dielectric constant of ionic solutions (79, 91–93). Recent work by Chen et al. further confirms our results showing that below 10 Å, water molecules change their orientational distribution from 10° to 20° per molecule even for highly diluted electrolyte solutions (below 0.1 M) (94).

To examine this effect, we categorize water molecules in solution into two distinct types (74), using the previously established nomenclature: hydrated water molecules belonging to the first hydration shell and free water molecules comprising all others. This framework allows us to treat the system as a binary mixture, where the water–water interaction energy can be expressed as

$$u_{ww} = \frac{U_{ww}}{N_w} = \frac{U_{hyd-hyd}}{N_w} + \frac{U_{hyd-free}}{N_w} + \frac{U_{free-free}}{N_w}, \qquad [1]$$

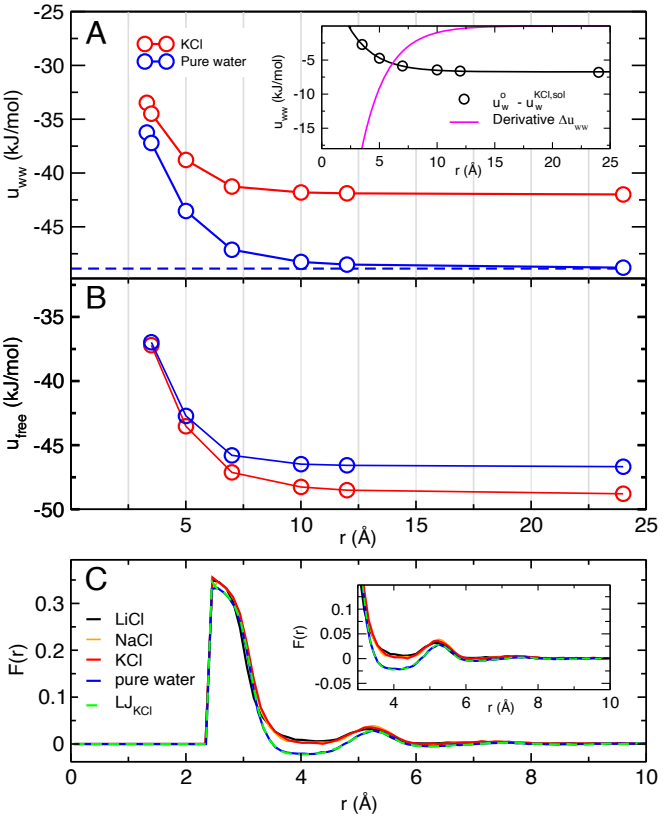

Fig. 5. (*A*) Water–water energy (Eq. **1**) as a function of the cutoff distance for the interaction potential at 283 K and 1 bar. The KCl solution is 1 m (mol/kg). The horizontal dashed line is the value of the energy of pure water u_{ww}^0 obtained by using Ewald sums (it is a constant shown only to illustrate that the energy is well converged at about 15 Å). The *Inset* shows the water–water energy difference between pure water and water in 1 m KCl solution (fitted with a spline) and its derivative. (*B*) Free water energy (Eqs. **1** and **2**) for the 1 m KCl solution compared to the energy of pure water. (*C*) Radial dipole–dipole spatial correlation function F(r) (as defined in ref. 90, which provides the average of the cosine of the angles between water dipoles at a distance *r*) at 283 K for 1 m chlorides using the Madrid-2019 model (36). The hydrophobic LJ_{KCl} (see text) is also included.

where U_{ww} is the total water–water energy, N_w the total number of water molecules, $U_{hyd-hyd}$ stands for the energy between molecules of water within the first hydration shell of the ions, $U_{free-free}$ is the energy between free water molecules, and $U_{hyd-free}$ is the crossed energy between free and hydrated water molecules. Assuming that the energy from the crossed interaction (*hyd-free*) can be equally distributed:

$$u_{ww} = \frac{N_{hyd}}{N_w}\left(\frac{U_{hyd-hyd} + \frac{1}{2}U_{hyd-free}}{N_{hyd}}\right) + \frac{N_{free}}{N_w}\left(\frac{U_{free-free} + \frac{1}{2}U_{hyd-free}}{N_{free}}\right) = x_{hyd}u_{hyd} + x_{free}u_{free} \quad [2]$$

For the 1 m solutions studied in this work, the typical molar fraction of free water molecules is around $x_{free} = 0.78$ to 0.80. Note that, as previously discussed in Table 2, free water exhibits the same number of hydrogen bonds as pure water for all the considered solutions. However, u_{free} also includes a contribution from hydrated molecules as defined in Eq. **2**. Fig. 5*B* shows that u_{free} mirrors the behavior of pure water up to 5 Å for KCl, after which it diverges and reaches a plateau at approximately 12 Å (the convergence distance for pure water and water in the solution). This indicates that dipole–dipole correlations are severely affected due to orientational rearrangements imposed by the ions, causing an energetically less favorable interaction compared to pure water. To confirm this speculation, we present in panel Fig. 5*C* the radial dipole–dipole correlation F(r) (90), which provides the average of the cosine of the angles between water dipoles at a distance r [all the water molecules of the system were considered when computing F(r)]. Not surprisingly, the LJ_{KCl} has no effect upon dipole–dipole correlations, as was deduced by the absence in the energy change ($\Delta u_{ww} \approx 0$), whereas there are notable changes in F(r) beyond 3.3 Å for ionic solutions, which again, increase with the charge density of the ions.

Table 4. Ions-water potential energy (in kJ/mol) for the different 1 m salt solutions at 283 K and p = 1 bar for the Madrid-2019 model

	u_{w-ions}(kJ/mol$_{water}$)	u_{w-ions}(kJ/mol$_{salt}$)
LiCl (aq)	−18.1	−1003
NaCl (aq)	−15.2	−842
KCl (aq)	−13.2	−730
CsCl (aq)	−12.3	−680

Finally, we must account for the ion–water interaction energy in the solutions (details provided in *SI Appendix*, section 6). Table 4 presents these results, where differences among salts reflect the influence of distinct cations on ion–water energetics, given that all salts share the same anion. Consistent with previous observations, the magnitude of ion–water interaction energy increases (in absolute value) as the cation size decreases.

Viscosity. The relationship between ionic perturbations of water structure and their influence on solution viscosity remains a subject of ongoing debate in physical chemistry. Although these two phenomena are fundamentally distinct, one representing an equilibrium structural property and the other a nonequilibrium transport coefficient, they were connected through the empirical equation proposed by Jones and Dole (80) to describe the variation of the viscosity in electrolyte solutions:

$$\eta/\eta_w = 1 + A\sqrt{m} + Bm, \quad [3]$$

where η and η_w denote the viscosities of the solution and pure water, respectively, m is the molality, A is related to long-range electrostatic interactions and can be theoretically estimated and B is a salt-dependent contribution which can be divided into ion-specific parameters. The traditional interpretation, originating from the work of Cox and Wolfenden (66), associates positive B values with structure-making ions that enhance water's hydrogen bond network and negative B values with structure-breaking ions that disrupt it. This classification draws an analogy with pressure-induced viscosity changes (9, 95), where compression reduces viscosity, which was refuted by Zhang et al. pointing to their different structural origins (75).

Concerning the influence of ions on water properties beyond the first hydration shell, it has been suggested that water maintains dynamics (32, 73, 89, 95), dipole moments (30), and has HB networks comparable to bulk water (75). Nevertheless, the energetic properties are substantially perturbed beyond the first hydration shell because of the orientation (not the magnitude) of the dipoles.

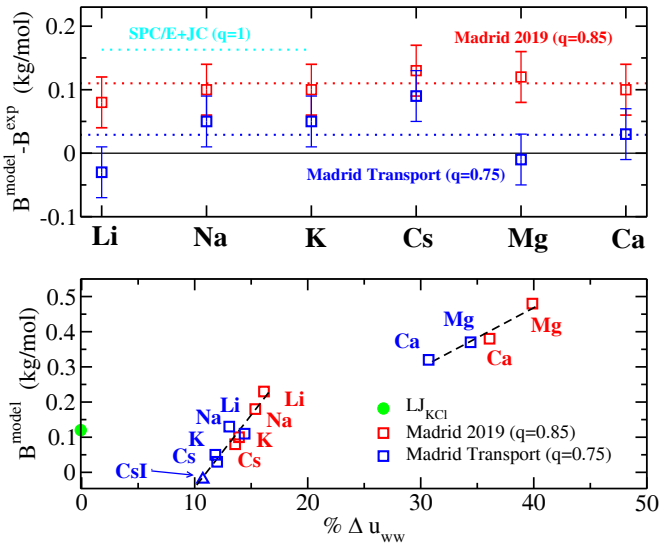

Fig. 6. *Top* panel Difference between the Jones-Dole coefficient, B (Eq. **3**) of several chlorides with the Madrid-2019 and Madrid Transport models (36, 101) compared to experimental values from ref. 98 at 298.15 and 1 bar. Dotted lines are the average deviation for each model as indicated in the legend. The data from SPC/E+JC has been taken from ref. 96 and estimating the average error of all monovalent halides studied there. *Bottom* panel Jones-Dole viscosity coefficient at 298.15 K (Eq. **3**) for the two models studied in this work (36, 101) as indicated in the legend and for the LJ_{KCl} particle (see text) vs. the percentage of the energy loss of water–water interactions in the solution compared to pure water (Eq.**1**). Black lines are fits using the data of both models for monovalent and divalent solutions. Chlorides are represented by squares. The cesium iodide is indicated by a triangle. Red symbols: Madrid-2019. Blue symbols: Madrid-transport.

In our systematic analysis, we have shown that all salts are detrimental to the water–water energy, including both classical structure-makers (e.g., LiCl, $B > 0$) and structure-breakers (e.g., CsCl, $B < 0$). Notably, LiCl induces the most substantial structural disruption despite its classification as a structure-maker, while CsCl, a structure-breaker, produces a smaller yet still significant effect.

Computational studies of the Jones-Dole B coefficient are a *tour de force* and have only been carried out by Yue and Panagiotopoulos (96, 97). The coefficients A and B are obtained typically (both in experiments and simulations) by plotting $(\eta/\eta_w - 1)/\sqrt{m}$ vs. $\sqrt{m}$. Low concentrations are needed so that Eq. **3** is valid and quadratic contributions can safely be neglected (*SI Appendix*, Eqs. S7–S9). Coefficients A and B are then obtained from the intercept and slope of a linear fit. Notice that diluted systems require extremely long simulations. In this work, we employ an approximate (but reasonable) procedure to estimate the value of the B coefficient. All the details are presented in *SI Appendix*, section 7. Since A is an order of magnitude smaller than B, we take it from experiments (98). B can then be approximated using a single concentration. Therefore, we use 1 m concentration for 1:1 electrolyte solutions and 0.6 m for 2:1 electrolyte solutions (to avoid hydrated ion-hydrated ion interactions from contributing to the calculated B coefficients). We have tested this approach using experimental viscosity values (99, 100), finding that the resulting B coefficients are within 0.01 kg/mol of those reported by Marcus (98) (*SI Appendix*, Table S9).

First, in Fig. 6*Top* panel we evaluate the quality of fixed-charge force fields to predict the experimental B values. We include results for the Madrid-2019 model (36) (which uses a scaled charge of q = 0.85) and the Madrid-Transport model (with q = 0.75) (101). The latter, which was originally developed for NaCl and KCl, has been extended in this work for other ions (namely, Li^+, Cs^+, Mg^{2+}, Ca^{2+}, and I^-). Details about this extension of the Madrid-Transport force field to these ions is provided in *SI Appendix*, Table S11. We observe that, as the value of the scaled charge used in the force field decreases, the predicted B coefficients get closer to the experimental values. To extend the discussion, we include the mean deviation of monovalent halides for the SPC/E (102)+JC (103) potential (that uses q = 1 for the ions) taken from ref. 96. This model deviates around 0.16 from experiments, whereas for scaled charge models, average deviations are 0.11, 0.03 (for q = 0.85 and 0.75, respectively). Furthermore, the error of 0.16 for the case q = 1 does not consider divalent cations, for which higher deviations are expected. Panel (*B*) shows the computed B coefficients for the two models vs. the water–water energy loss in 1 m chloride solutions. Additionally, we have included the CsI, which presents (for the Madrid-transport model) a negative B coefficient. To the best of our knowledge, previous fixed-charge force fields have been unable to attain negative Jones-Dole coefficients. We observe a correlation between B and Δu_{ww}, which is independent of the model used, although displaying different trends for monovalent and divalent ions. This is also observed in experiments when the Jones-Dole coefficient is represented against the partial molar entropies (*SI Appendix*, Fig. S10) (67). Fig. 6*Bottom* panel shows that all ions are structure breakers when one considers the water–water energy regardless of the B coefficient.

To further assess the relationship between viscosity and energy loss, we now look at the total energy of the water in solution (u_w^{sol}); that is, including its interaction with the ions (Table 4). Again, we must assume that half of the ion–water interaction can be ascribed to water.

$$u_w^{sol} = U_{ww}/N_w + 1/2(U_{w-ion}/N_w);$$
$$\Delta u_w = u_w^{sol} - u_w^0 \qquad [4]$$

In Fig. 7*A*, we represent the B coefficients of the two models considered in this work vs. the energy difference between water in solution and pure water (including the interaction between water and ions as established in Eq. **4**). A clear linear correlation exists between these two properties, now encompassing both monovalent and divalent chlorides. To further test the universality of this correlation, we have extended the calculations beyond chlorides, including CsI and the LJ_{KCl} hydrophobic particle, which also follow this trend (notice that the small water–LJ solute energy contribution was incorporated when computing the energy of water in solution in this case). Therefore, the energy of water provides a simple structural explanation of the value of B for a wide range of systems. For the model with q = 0.75, which describes reasonably well (although not perfectly) the experimental values of B, the change of sign of B occurs when Δu_w adopts a small and positive value, namely 0.75 kJ/mol. For larger positive values of Δu_w, the value of B becomes negative and the salt can be denoted as structure breaker, which now seems a proper descriptive notation since, in fact, the energy of water in solution is larger than that of pure water.

Despite the small deviation from experimental B coefficients provided by the Madrid-Transport, fixed-charged models are still unable to completely describe the complex dynamic behavior of electrolyte solutions (65, 97), being the electronic heterogeneity (and also the presence of nuclear quantum effects) paramount for describing these phenomena (77, 87, 104, 105). However, some of these models are successful in describing the changes in the TMD due to the presence of salt (60, 61), as well as the equation

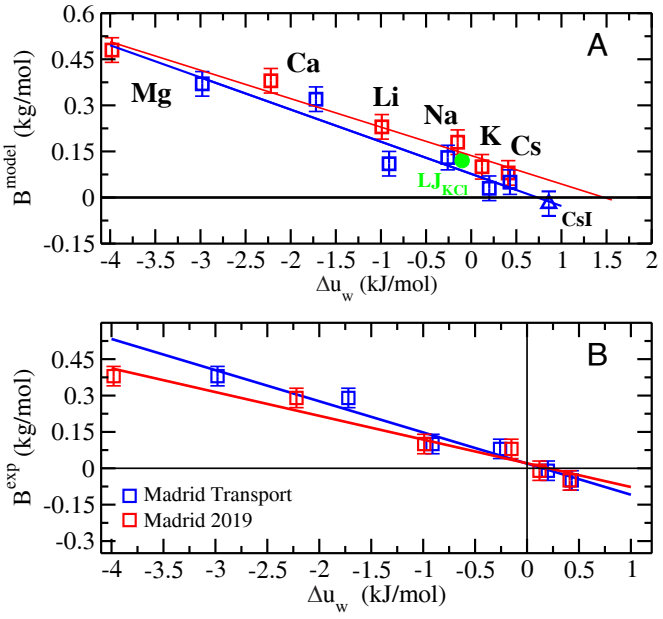

Fig. 7. (*A*) Jones-Dole coefficient vs. the energy difference of water in solution (Δu_W, see Eq. **4**) and pure water (u_w^0) for 1 m chloride solutions at 298 K and 1 bar using the Madrid Transport (blue) (101) and the Madrid-2019 (36) (red) force fields. The green point corresponds to the LJ_{KCl} particle (see text). The cesium iodide (triangle) is not included in the fit. (*B*) Experimental Jones-Dole coefficient vs. the energy difference of water in solution for two different models as indicated in the legend. Coloured solid lines are linear fits to the models.

of state and compressibility at moderate pressures (63), so that they are reliable for structural changes. Thus, one can tentatively combine the experimental values of B with the energy change of water, Δu_w, using those models in a single plot. This is shown in Fig. 7*B*. The change of sign of B in this plot occurs when $\Delta u_w =$ 0.25 kJ/mol, a value somewhat closer to zero. While Fig. 7*B* must be treated cautiously because it combines experimental B values with modeled Δu_w values, its results are consistent with those in Fig. 7*A*, which uses simulation data for both parameters. For both models, the change of sign of B occurs when the energy of water in the solution is similar (although slightly larger) than that of pure water. This finding helps bring coherence to the terms structure making/breaking from an energetic point of view.

At this point, it is worthwhile to revisit an interpretation given in the classic Jones-Dole paper (80): "Applebey made the suggestion that when a salt is dissolved in water there are two different effects on the viscosity: 1) a depolymerization of triple water molecules $(H_2O)_3$ to form single molecules, which tends to diminish the viscosity; 2) an increase in viscosity due to the presence of the ions of the salt." In modern terms, contribution (1) can be understood as the breaking of hydrogen bonds and the disruption of dipole–dipole correlations between water molecules, which destabilizes water–water interactions. Contribution (2), in turn, relates to the electrostriction imposed by the ions (where the ion–water interaction stabilizes water). Fig. 7 in this work illustrates the combined effect of both contributions. When contributions (1) and (2) are comparable in magnitude, they partially cancel each other out. As a result, the ions do not significantly modify the viscosity and, consequently, the dynamics of water (81).

Discussion

We have investigated the structure and energetics of water in 1 m chloride solutions using a well-validated nonpolarizable model (36). Our findings reveal that water molecules surrounding the anion do not orient their dipole moments along the Cl-O vector, as the energetic benefit of forming hydrogen bonds with the anion outweighs that of dipole alignment with the anion's electric field. Conversely, water dipoles orient in the opposite direction around the cations, with interaction strength inversely related to cation size. Structural features of the solutions are quantified using the KL-divergence and local entropy calculations. Analysis of hydrogen bond (HB) networks shows that approximately 5% of the total HBs (between water molecules) are lost for 1 m solutions, being this breakage strictly localized within the first hydration shell of ions, with free water maintaining the normal number of HBs. However, the total energy loss between water molecules in the solution ranges between 13.5 to 16%, with the percentage difference between HB and energy loss attributable to altered orientational correlations between water molecules, which significantly impact dipole interaction energies. Our results challenge the traditional structure-making/breaking dichotomy, as we observe that all ions disrupt the hydrogen bonding network. Although free water preserves its HB almost intact, the hydrated water molecules are unable to form HB with each other around Li^+. This constraint diminishes as the cation size increases. By analyzing energetics rather than poorly defined "structure," we establish a correlation between viscosity B coefficients and the energy of water in the solution. When this energy (including the ion contribution) is higher than that of pure water (by about 0.5 kJ/mol), negative values of B are expected. This correlation holds universally for chloride salts, including divalent ions and also for CsI and a hydrophobic particle.

Materials and Methods

Molecular dynamics simulations were conducted using GROMACS 4.6.7 (106) (double precision) in the *NpT* ensemble and using 2 fs as the time step. Temperature and pressure were regulated via the Nose–Hoover thermostat (107, 108) and the Parrinello–Rahman barostat (109) respectively, both with relaxation times of 2 ps. The interactions between water molecules were modeled using the rigid, nonpolarizable TIP4P/2005 water model (110), while ions were parameterized with the Madrid-2019 force field (36), specifically optimized for TIP4P/2005. A cutoff radius of 1 nm was employed for both the dispersive and the real-space components of electrostatic interactions. Long-range electrostatic interactions were computed using the Particle Mesh Ewald (PME) method, with standard long-range corrections applied to the Lennard-Jones energies and pressures. Water molecule geometries were constrained using the LINCS algorithm (111). Periodic boundary conditions were applied in all three spatial dimensions. Simulations were performed for small (555 water molecules) and big (4,440 water molecules) systems in cubic boxes with the appropriate number of ions added to achieve concentration of 1 molal (1 mol of salt per kg of water). Runs of 150 and 15 ns were performed for small/large systems respectively, with appropriate equilibration periods excluded from the analysis. All the structural properties were obtained at 283 K and 1 bar. The energy calculations were also done at 298.15 K (as indicated for each case) and the aforementioned simulation details. Results with Madrid-Transport (q = 0.75) (101) are also reported (*SI Appendix*). This model has been extended in this work for Li^+, Cs^+, Mg^{2+}, Ca^{2+}, and I^-. The parameters can be found in *SI Appendix*, section S8. Viscosity calculations were performed in the NVT ensemble at 298.15 K with the same setup (more details are provided in *SI Appendix*, section S7). Unless otherwise stated, all the results from figures and tables were obtained with the Madrid-2019 at 283 K and 1 bar. A custom-built (free) software: ANGULA (112) was used for the structural analysis, including the KL-divergence and entropies (*SI Appendix*).

Data, Materials, and Software Availability. The ANGULA software is available at https://gcm.upc.edu/en/members/luis-carlos/angula/ANGULA (112).

Additionally, the topology files for the Madrid-2019 and the Madrid-Transport models used in this work can be found in Zenodo https://doi.org/10.5281/zenodo.18685416 (113). All other data are included in the manuscript and/or *SI Appendix*.

ACKNOWLEDGMENTS. This work was supported by the MCIN Projects PID2020-112975GB-I00, TED2021-130265B-C22, PID2022-136919NB-C31, PID2025-168591NB-I00 and before this project acknowledge Ministerio de Ciencia Innovación y Universidades (MICIU) and also European Regional Development Fund and European Union PID2023-151751NB-I00 MICIU/AEI/10.13039/501100011033, by the Dirección General de Universidades Project 2021SGR-00343 (Catalonia) and Maria de Maeztu project CEX2023-001300-M/funded by MCIN/AEI/10.13039/501100011033. L.F.S. acknowledges the Ministerio de Ciencia e Innovación (MCIN) for a predoctoral Formación de Profesorado Universitario under Grant No. FPU22/02900.

Author affiliations: [a]Departamento de Química Física, Facultad de Ciencias Químicas, Universidad Complutense de Madrid, Madrid 28040, Spain; [b]Group of Characterization of Materials, Department of Physics, Engineering School of Barcelona, Universitat Politecnica de Catalunya, Barcelona 08019, Spain; [c]Department of Physics and Barcelona Research Center in Multiscale Science and Engineering, Universitat Politecnica de Catalunya, Barcelona 08019, Spain; and [d]Instituto de Química Física Blas Cabrera, Consejo Superior de Investigaciones Científicas, Madrid 28006, Spain

1. H. K. Manji, W. C. Drevets, C. A. Zarate, The cellular and molecular mechanisms of action of lithium in the treatment of bipolar disorder. *Eur. Neuropsychopharmacol.* **13**, 385–394 (2003).
2. M. V. L. Bennett, S. B. Kater, Sodium and potassium in muscle contraction. *Annu. Rev. Physiol.* **38**, 227–246 (1976).
3. F. Fuchs, M. Gable, The role of sodium and potassium in muscle contraction. *Physiol. Rev.* **65**, 677–711 (1985).
4. D. S. Adams, M. Levin, Endogenous voltage gradients as mediators of cell-cell communication: Strategies for investigating bioelectrical signals during pattern formation. *Cell Tissue Res.* **352**, 95–122 (2013).
5. M. Levin, Endogenous bioelectrical networks store non-genetic patterning information during development and regeneration. *J. Physiol.* **592**, 2295–2305 (2014).
6. H. Ohtaki, T. Radnai, Structure and dynamics of hydrated ions. *Chem. Rev.* **3**, 1157–1204 (1993).
7. G. W. Neilson, J. E. Enderby, Chapter 7. Neutron and X-ray diffraction studies of concentrated aqueous electrolyte solutions. *Annu. Rep. Prog. Chem. Sect. C Phys. Chem.* **76**, 185–220 (1979).
8. R. H. Tromp, G. W. Neilson, A. K. Soper, Water structure in concentrated lithium chloride solutions. *J. Chem. Phys.* **96**, 8460–8469 (1992).
9. H. D. B. Jenkins, Y. Marcus, Viscosity B-coefficients of ions in solution. *Chem. Rev.* **95**, 2695 (1995).
10. Y. Marcus, Viscosity B-coefficients, structural entropies and heat capacities, and the effects of ions on the structure of water. *J. Solut. Chem.* **23**, 831–848 (1994).
11. Y. Marcus, Effect of ions on the structure of water: Structure making and breaking. *Chem. Rev.* **109**, 1346–1370 (2009).
12. A. W. Omta, M. F. Kropman, Woutersen, Influence of ions on the hydrogen-bond structure in liquid water. *J. Chem. Phys.* **119**, 12457 (2003).
13. R. Mancinelli, A. Botti, F. Bruni, M. A. Ricci, A. K. Soper, Hydration of sodium, potassium, and chloride ions in solution and the concept of structure maker/breaker. *J. Phys. Chem. B* **111**, 13570–13577 (2007).
14. I. Waluyo *et al.*, The structure of water in the hydration shell of cations from X-ray Raman and small angle X-ray scattering measurements. *J. Chem. Phys.* **134**, 064513 (2011).
15. I. Waluyo *et al.*, Increased fraction of low-density structures in aqueous solutions of fluoride. *J. Chem. Phys.* **134**, 224507 (2011).
16. R. J. Copper, T. M. Chang, E. R. Williams, Hydrated alkali metal ions: Spectroscopic evidence for clathrates. *J. Phys. Chem. A* **117**, 6571–6579 (2013).
17. K. A. Perrine *et al.*, Specific cation effects at aqueous solution vapor interfaces: Surfactant like behavior of Li^+ revealed by experiments and simulations. *Proc. Natl. Acad. Sci. U.S.A.* **114**, 13363–13368 (2017).
18. U. Farooq *et al.*, Microsolvation of salts in water: A comprehensive overview of the experimental and computational approaches. *Coord. Chem. Rev.* **517**, 216041 (2024).
19. A. Botti, S. E. Pagnotta, F. Bruni, M. A. Ricci, Solvation of KSCN in water. *J. Phys. Chem. B* **113**, 10014–10021 (2009).
20. J. D. Smith, R. J. Saykally, P. L. Geissler, The effects of dissolved halide anions on hydrogen bonding in liquid water. *J. Am. Chem. Soc.* **129**, 13847–13856 (2007).
21. J. C. Deak, S. T. Rhea, L. K. Iwaki, D. D. Dlott, Vibrational energy transfer across a reverse micelle surfactant layer. *J. Phys. Chem. A* **104**, 4866 (2000).
22. H. Graener, T. Q. Ye, A. Laubereau, Ultrafast dynamics of hydrogen bonds directly observed by time-resolved infrared spectroscopy. *J. Chem. Phys.* **90**, 3413 (1988).
23. V. Balos *et al.*, Time-resolved terahertz-Raman spectroscopy reveals that cations and anions distinctly modify intermolecular interactions of water. *Nat. Chem.* **14**, 1031–1037 (2022).
24. M. Flor *et al.*, Unraveling the molecular pathways for structure "making" and "breaking" by ions in water. *J. Am. Chem. Soc.* **147**, 37328–37336 (2025).
25. J. Chandrasekhar, W. L. Jorgensen, The nature of dilute solutions of sodium ion in water, methanol, and tetrahydrofuran. *J. Chem. Phys.* **77**, 5080–5089 (1982).
26. M. T. H. Nguyen, O. Tichacek, H. Martinez-Seara, P. E. Mason, P. Jungwirth, Resolving the equal number density puzzle: Molecular picture from simulations of licl(aq) and nacl(aq). *J. Phys. Chem. B* **125**, 3153–3162 (2021).
27. A. P. Gaiduk, C. Zhang, F. Gygi, G. Galli, Structural and electronic properties of aqueous NaCl solutions from ab initio molecular dynamics simulations with hybrid density functionals. *Chem. Phys. Lett.* **604**, 89–96 (2014).
28. P. Gallo, M. Martin Conde, D. Corradini, P. Pugliese, M. Rovere, *Structural Properties of Ionic Aqueous Solutions*, G. Angilella, C. Amovilli, Eds. (Springer International Publishing, Cham, 2018), pp. 153–162.
29. A. Lyubarstev, K. Laasonen, A. Laaksonen, Hydration of Li^+ ion. An ab initio molecular dynamics simulation *J. Chem. Phys.* **114**, 3120 (2001).
30. R. Savoj, H. Agnew, R. Z. F. Paesani, Molecular insights into the influence of ions on the water structure. I. Alkali metal ions in solution. *J. Phys. Chem. B* **128**, 1953–1962 (2024).
31. E. Pluharova, P. Jungwirth, N. Matubayasi, O. Marsalek, Structure and dynamics of the hydration shell: Spatially decomposed time correlation approach. *J. Chem. Theory Comput.* **15**, 802–812 (2019).
32. G. Stirnemann, E. Wernersson, P. Jungwirth, D. Laage, Mechanisms of acceleration and retardation of water dynamics by ions. *J. Am. Chem. Soc.* **135**, 11824–11831 (2013).
33. J. Dockal, M. Lísal, F. Moucka, Molecular force field development for aqueous electrolytes: 2. polarizable models incorporating crystalline chemical potential and their accurate simulations of halite, hydrohalite, aqueous solutions of NaCl, and solubility. *J. Chem. Theory Comp.* **16**, 3677-3688 (2020).
34. A. Grossfield, P. Ren, J. W. Ponder, Ion solvation thermodynamics from simulation with a polarizable force field. *J. Am. Chem. Soc.* **125**, 15671–15682 (2003).
35. P. T. Kiss, A. Baranyai, A new polarizable force field for alkali and halide ions. *J. Chem. Phys.* **141**, 114501 (2014).
36. I. Zeron, J. L. F. Abascal, C. Vega, A force field of Li^+, Na^+, K^+, Mg^{2+}, Ca^{2+}, Cl^-, and SO_4^{2-} in aqueous solution based on the TIP4P/2005 water model and scaled charges for the ions *J. Chem. Phys.* **151**, 134504 (2019).
37. R. Fuentes-Azcatl, M. C. Barbosa, Sodium chloride, NaCl/ϵ: New force field. *J. Phys. Chem. B* **120**, 2460–2470 (2016).
38. Z. Kann, J. L. Skinner, A scaled-ionic-charge simulation model that reproduces enhanced and suppressed water diffusion in aqueous salt solutions. *J. Chem. Phys.* **141**, 104507 (2014).
39. T. Yagasaki, M. Matsumoto, H. Tanaka, Lennard-Jones parameters determined to reproduce the solubility of nacl and kcl in spc/e, tip3p, and TIP4P/2005 water. *J. Chem. Theory Comput.* **14**, 2460–2473 (2020).
40. M. Kohagen, P. E. Mason, P. Jungwirth, Accurate description of calcium solvation in concentrated aqueous solutions. *J. Phys. Chem. B* **118**, 7902–7909 (2014).
41. M. Kohagen, P. E. Mason, P. Jungwirth, Accounting for electronic polarization effects in aqueous sodium chloride via molecular dynamics aided by neutron scattering. *J. Phys. Chem. B* **120**, 1454–1460 (2015).
42. L. Le, V. Molinero, Nanophase segregation in supercooled aqueous solutions and their glasses driven by the polyamorphism of water. *J. Phys. Chem. A* **115**, 5900–5907 (2011).
43. R. C. DeMille, V. Molinero, Coarse-grained ions without charges: Reproducing the solvation structure of NACL in water using short-ranged potentials. *J. Chem. Phys.* **131**, 034107 (2009).
44. C. Krekeler, B. Hess, L. Delle Site, Density functional study of ion hydration for the alkali metal ions and the halide ions. *J. Chem. Phys.* **125**, 054305 (2006).
45. S. Varma, S. B. Rempe, Coordination numbers of alkali metal ions in aqueous solutions. *Biophys. Chem.* **124**, 192–199 (2006).
46. Y. Yao, Y. Kanai, Free energy profile of nacl in water: First-principles molecular dynamics with scan and ωb97x-v exchange-correlation functionals. *J. Chem. Theory Comput.* **14**, 884–893 (2018).
47. M. J. Field, P. A. Bash, M. Karplus, A combined quantum mechanical and molecular mechanical potential for molecular dynamics simulations. *J. Comput. Chem.* **11**, 700–733 (1990).
48. A. Tongraar, K. R. Liedl, B. M. Rode, Born-oppenheimer ab initio QM/MM dynamics simulations of Na^+ and K^+ in water: from structure making to structure breaking effects *J. Phys. Chem. A* **102**, 10340–10347 (1998).
49. B. Lier *et al.*, Buffer region neural network approach for polarizable- embedding neural network/molecular mechanics simulations. *J. Phys. Chem. Lett.* **13**, 3812–3818 (2022).
50. I. V. Leontyev, A. A. Stuchebrukhov, Electronic continuum model for molecular dynamics simulations. *J. Chem. Phys.* **130**, 085102 (2009).
51. I. V. Leontyev, A. A. Stuchebrukhov, Electronic polarizability and the effective pair potentials of water. *J. Chem. Theory Comput.* **6**, 3153–3161 (2010).
52. F. Moučka, I. Nezbeda, W. R. Smith, Molecular force field development for aqueous electrolytes: 1. Incorporating appropriate experimental data and the inadequacy of simple electrolyte force fields based on Lennard-Jones and point charge interactions with Lorentz-Berthelot rules. *J. Chem. Theory Comput.* **9**, 5076–5085 (2013).
53. M. Soniat, S. W. Rick, Charge transfer effects of ions at the liquid water/vapor interface. *J. Chem. Phys.* **140**, 184703 (2014).
54. M. Soniat, G. Pool, L. Franklin, S. W. Rick, Ion association in aqueous solution. *Fluid Phase Equilib.* **407**, 31–38 (2016).
55. S. Blazquez, M. M. Conde, J. L. Abascal, C. Vega, The madrid-2019 force field for electrolytes in water using TIP4P/2005 and scaled charges: Extension to the ions f^-, br^-, i^-, rb^+, and cs^+ *J. Chem. Phys.* **156**, 044505 (2022).
56. E. Dubouè-Dijon, M. Javanainen, P. Delcroix, P. Jungwirth, H. Martinez-Seara, A practical guide to biologically relevant molecular simulations with charge scaling for electronic polarization. *J. Chem. Phys.* **153**, 050901 (2020).
57. G. Le Breton, L. Joly, Molecular modeling of aqueous electrolytes at interfaces: Effects of long-range dispersion forces and of ionic charge rescaling. *J. Chem. Phys.* **152**, 241102 (2020).
58. V. Kostal, P. E. Mason, H. Martinez-Seara, P. Jungwirth, Common cations are not polarizable: Effects of dispersion correction on hydration structures from ab initio molecular dynamics. *J. Phys. Chem. Lett.* **14**, 4403–4408 (2023).
59. A. Chattopadhyay, V. Mandalaparthy, N. F. A. van der Vegt, Determination of aqueous solubility of NaCl in molecular dynamics simulation using the Kirkwood-Buff method. *J. Chem. Phys.* **162**, 174116 (2025).
60. L. F. Sedano, S. Blazquez, E. G. Noya, C. Vega, J. Troncoso, Maximum in density of electrolyte solutions: Learning about ion-water interactions and testing the Madrid-2019 force field. *J. Chem. Phys.* **156**, 154502 (2022).

61. F. Gamez, L. F. Sedano, S. Blazquez, J. Troncoso, C. Vega, Building a Hofmeister-like series for the maximum in density temperature of aqueous electrolyte solutions. *J. Molec. Liq.* **337**, 121433 (2023).
62. C. P. Lamas, C. Vega, E. G. Noya, Freezing point depression of salt aqueous solutions using the Madrid-2019 model. *J. Chem. Phys.* **156**, 134503 (2022).
63. L. F. Sedano, C. Vega, E. G. Noya, Isothermal compressibility and water self-diffusion coefficient in supercooled salt aqueous solutions using the Madrid-2019 model. *Mol. Phys.* **122**, e2418311 (2024).
64. P. Garbacz, W. S. Price, 1H NMR diffusion studies of water self-diffusion in supercooled aqueous sodium chloride solutions. *J. Phys. Chem. A* **118**, 3307 (2014).
65. J. S. Kim, W. Zhe, A. R. Morrow, A. Yethiraj, A. Yethiraj, Self-diffusion and viscosity in electrolyte solutions. *J. Phys. Chem.* **116**, 12007–12013 (2012).
66. W. M. Cox, J. H. Wolfenden, The viscosity of strong electrolytes measured by a differential method. *Proc. R. Soc. A* **475**, 145 (1934).
67. R. W. Gurney, *Ionic Processes in Solution* (McGraw Hill, New York, 1953).
68. F. Hofmeister, Zur lehre von der wirkung der salze. *Arch. Exp. Pathol. Pharmakol.* **24**, 247–260 (1888).
69. O. Samoilov, A new approach to the study of hydration of ions in aqueaous solutions. *Discuss. Faraday Soc.* **24**, 141,146 (1957).
70. H. Peng, A. V. Nguyen, A link between viscosity and cation-anion contact pairs: Adventure on the concept of structure-making/breaking for concentrated salt solutions. *J. Mol. Phys.* **263**, 109–117 (2018).
71. B. Hribar, N. T. Southall, V. Vlachy, K. A. Dill, How ions affect the structure of water. *J. Am. Chem. Soc.* **124**, 12302–12311 (2002).
72. K. D. Collins, G. W. Neilson, J. E. Enderby, Ions in water: Characterizing the forces that control chemical processes and biological structure. *Biophys. Checm.* **128**, 95 (2007).
73. R. Shi, A. J. Cooper, H. Tanaka, Impact of hierarchical water dipole orderings on the dynamics of aqueous salt solutions. *Nat. Commun.* **14**, 4616 (2023).
74. J. Chandrasekhar, D. C. Spellmeyer, W. L. Jorgensen, Energy component analysis for dilute aqueous solutions of Li^+, Na^+, F^- and Cl^- ions *J. Am. Chem. Soc.* **106**, 903–910 (1984).
75. C. Zhang, S. Yue, A. Z. Panagiotopoulos, M. L. Klein, X. Wu, Dissolving salt is not equivalent to applying a pressure on water. *Nat. Commun.* **13**, 822 (2022).
76. P. B. Balbuena, K. P. Johnston, P. J. Rossky, Molecular dynamics simulation of electrolyte solutions in ambient and supercritical water. 1. Ion solvation. *J. Phys. Chem.* **100**, 2706–2715 (1996).
77. Y. Ding, A. A. Hassanali, M. Parrinello, Anomalous water diffusion in salt solutions. *Proc. Natl. Acad. Sci. U.S.A.* **111**, 3310–3315 (2014).
78. X. Wang *et al*., Density functional theory based molecular dynamics study of solution composition effects on the solvation shell of metal ions. *Phys. Chem. Chem. Phys.* **22**, 16301 (2020).
79. C. Zhang *et al*., Why dissolving salt in water decreases its dielectric permittivity. *Phys. Rev. Lett.* **131**, 076801 (2023).
80. G. Jones, M. Dole, The viscosity of aqueous solutions of strong electrolytes with special reference to barium chloride. *J. Am. Chem. Soc.* **51**, 2950 (1929).
81. D. W. McCall, D. C. Douglass, The effect of ions on the self-diffusion of water. I. Concentration dependence. *J. Phys. Chem.* **69**, 2001 (1965).
82. M. C. Despretz, Reserches sur le maximum de densité des dissolutions aqueuses. *Ann. Chim. Phys.* **70**, 49 (1839).
83. M. Laliberte, W. E. Cooper, Model for calculating the density of aqueous electrolyte solutions. *J. Chem. Eng. Data* **49**, 1141–1151 (2004).
84. R. J. Cooper, J. M. Chang, E. R. Williams, Hydrated alkali metal ions: spectroscopic evidence for clathrates. *J. Phys. Chem. A* **117**, 6571–6579 (2013).
85. A. Luzar, D. Chandler, Hydrogen-bond kinetics in liquid water. *Nature* **379**, 55 (1996).
86. J. Grabowska, A. Kuffel, J. Zielkiewicz, Revealing the frank-evans "iceberg" structures within the solvation layer around hydrophobic solutes. *J. Phys. Chem. B* **125**, 1611–1617 (2021).
87. J. Liu, X. Zhou, X. He, Structure making and breaking effects of ions on the anomalous diffusion of water revealed by machine learning potentials. *Phys. Chem. Chem. Phys.* **27**, 12438 (2025).
88. R. Mancinelli, A. Botti, F. Bruni, M. A. Ricci, A. K. Soper, Perturbation of water structure due to monovalent ions in solution. *Phys. Chem. Chem. Phys.* **9**, 2959–2967 (2007).
89. A. W. Omta, M. F. Kropman, S. Woutersen, H. J. Bakker, Negligible effect of ions on the hydrogen-bond structure in liquid water. *Science* **301**, 347–349 (2003).
90. C. Zhang, G. Galli, Dipolar correlations in liquid water. *J. Chem. Phys.* **141**, 084504 (2014).
91. O. Blüh, Die dielektrizitätskonstanten von elektrolytlösungen. *Z. Phys.* **25**, 220 (1924).
92. J. B. Hasted, D. M. Ritson, C. H. Collie, Dielectric properties of aqueous ionic solutions. Parts I and II. *J. Chem. Phys.* **16**, 1 (1948).
93. R. Buchner, G. T. Hefter, P. M. May, Dielectric relaxation of aqueous nacl solutions. *J. Phys. Chem. A* **103**, 1 (1999).
94. Y. Chen *et al*., Electrolytes induce long-range orientational order and free energy changes in the h-bond network of bulk water. *Sci. Adv.* **2**, e1501891 (2016).
95. J. Holzmann, R. Ludwig, A. Geiger, D. Paschek, Pressure and salt effects in simulated water: Two sides of the same coin? *Angew. Chem.* **46**, 8907–8911 (2007).
96. S. Yue, A. Z. Panagiotopoulos, Dynamic properties of aqueous electrolyte solutions from non-polarisable, polarisable, and scaled-charge models. *Mol. Phys.* **117**, 3538–3549 (2019).
97. A. Z. Panagiotopoulos, S. Yue, Dynamics of aqueous electrolyte solutions: Challenges for simulations. *J. Phys. Chem. B* **127**, 430–437 (2023).
98. Y. Marcus, *Ion Properties* (Marcel Dekker Inc., 1997).
99. M. Laliberté, Model for calculating the viscosity of aqueous solutions. *J. Chem. Eng. Data* **52**, 321–335 (2007).
100. A. G. Ostroff, B. S. Snowden Jr., D. E. Woessner, Viscosities of protonated and deuterated water solutions of alkali metal chlorides. *J. Phys. Chem.* **73**, 2784 (1969).
101. S. Blazquez, M. M. Conde, C. Vega, Scaled charges for ions: An improvement but not the final word for modeling electrolytes in water. *J. Chem. Phys.* **158**, 054505 (2023).
102. H. J. C. Berendsen, J. R. Grigera, T. P. Straatsma, The missing term in effective pair potentials. *J. Phys. Chem.* **91**, 6269–6271 (1987).
103. I. S. Joung, T. E. Cheatham, Determination of alkali and halide monovalent ion parameters for use in explicitly solvated biomolecular simulations. *J. Phys. Chem. B* **112**, 9020–9041 (2008).
104. Y. Yao, M. L. Berkowitz, Y. Kanai, Communication: Modeling of concentration dependent water diffusivity in ionic solutions: Role of intermolecular charge transfer. *J. Chem. Phys.* **143**, 241101 (2015).
105. A. Z. Panagiotopoulos, Simulations of activities, solubilities, transport properties, and nucleation rates for aqueous electrolyte solutions. *J. Chem. Phys.* **153**, 010903 (2020).
106. B. Hess, C. Kutzner, D. V. der Spoel, E. Lindahl, Gromacs4: Algorithms for highly efficient, load-balanced and scalable molecular simulation. *J. Chem. Theory Comput.* **4**, 435–447 (2008).
107. S. Nosé, A molecular dynamics method for simulations in the canonical ensemble. *Mol. Phys.* **52**, 255–268 (1984).
108. W. G. Hoover, Canonical dynamics: Equilibrium phase-space distributions. *Phys. Rev. A* **31**, 1695–1697 (1985).
109. M. Parrinello, A. Rahman, Polymorphic transitions in single crystals: A new Molecular Dynamics method. *J. Appl. Phys.* **52**, 7182–7190 (1981).
110. J. L. F. Abascal, C. Vega, A general purpose model for the condensed phases of water: Tip4p/2005. *J. Chem. Phys.* **123**, 234505 (2005).
111. B. Hess, H. Bekker, H. J. C. Berendsen, J. G. E. M. Fraaije, Lincs: A linear constraint solver for molecular simulations. *J. Comput. Chem.* **18**, 1463 (1997).
112. L. C. Pardo, ANGULA software (2010). https://gcm.upc.edu/en/members/luis-carlos/angula/ANGULA. Accessed 22 February 2024.
113. L. F. Sedano, Topology (for gromacs) files for the Madrid-2019 (extended) and the Madrid-Transport electrolyte models with the TIP4P/2005 water model. https://doi.org/10.5281/zenodo.18685416. Deposited 18 February 2026.